Simultaneously measured vorticity and passive heat in a cylinder wake

H. Cao [1], T. Zhou [2*], Y. Zhou [1,3], H. Zhang [4]

[1]Shenzhen Graduate School, Harbin Institute of Technology,
University Town, Shenzhen, China,

[2]School of Civil and Resource Engineering, The University of Western Australia,
35 Stirling Highway, Crawley, WA 6009, Australia
Corresponding author: tongming.zhou@uwa.edu.au

[3]Department of Mechanical Engineering, The Hong Kong Polytechnic University,
Hung Hom, Kowloon, Hong Kong
[4]School of Measurement Technology and Engineering, China Jiliang University,
Hangzhou, China

INTRODUCTION

This work is an experimental study of the turbulent vortex structures, and momentum and heat transport in the intermediate wake of a slightly heated cylinder. Both coherent and incoherent vorticity fields are investigated using a phase-averaged technique. A circular cylinder with a diameter d=12.7mm was used to generate the wake. The free-stream velocity U_∞ was 3m/s, corresponding to a Reynolds number Re ($\equiv U_\infty d/\nu$) of 2540. The measurement locations are x/d=10, 20 and 40.The three components of vorticity vector were measured simultaneously using a multi-hot-wire probe (four cross-wires). Another cross-wire was used to provide a phase reference for the measured vorticity signals. The phase-averaged method is similar to that used by Matsumura et al. (1993) and Zhou et al. (2002).

RESULTS AND DISCUSSION

Figure 1 presents the iso-contours of phase-averaged coherent vorticity $\tilde{\omega}_x^*$, $\tilde{\omega}_y^*$ and $\tilde{\omega}_z^*$, where an asterisk denotes normalization by d and U_∞. The phase φ, ranging from -2π to 2π, can be interpreted in terms of a longitudinal distance; φ=2π corresponds to the average vortex wavelength λ. Note that the same scales are used in the φ and y^* directions in figure 1 and other figures that follow, to avoid any distortion of the physical space. The flow direction is from left to right in all figures.

The coherent spanwise vorticity $\tilde{\omega}_z^*$ at x/d=10 and 20 (figure 1g, h) display the well-known Kármán vortex street. The maximum concentration of $\tilde{\omega}_z^*$ decay from 1.3 at x/d=10 to 0.13 at x/d=40. The present data are in good agreement with Yiu and Zhou's estimate. This decay rate is much faster compared with $\tilde{\omega}_x^*$ and $\tilde{\omega}_y^*$ .The vortex street seems to have broken down at x/d=40(Fig.1i). The $|\tilde{\omega}_{z\max}^*|$ ratio of the positively signed vortex to that of the negative one is 1.08 at x/d=10 and drops to 0.59 at x/d=40. The vortex centre (maximum concentration of $\tilde{\omega}_z^*$) slowly shifts upwardly to the free stream with increasing x/d. The coherent lateral vorticity $\tilde{\omega}_y^*$ contours are not as distinct as $\tilde{\omega}_z^*$, and exhibit little connection to those of $\tilde{\omega}_z^*$. The coherent streamwise vorticity $\tilde{\omega}_x^*$ exhibits organized structures, with a much weaker strength than $\tilde{\omega}_z^*$. As vortices move downstream, $\tilde{\omega}_x^*$ and $\tilde{\omega}_y^*$ disperse in the lateral direction (y) more rapidly than $\tilde{\omega}_z^*$.

Contours of phase-averaged coherent heat fluxes are shown in figure 2a-f (x/d=10 and 20). In the case of $\tilde{u}^*\tilde{\theta}^*$ (figure 2a, b) the positive contour is dominant when y^*>0. Near the centreline, there are several negative contours when y^* <0. This trend becomes more pronounced at x/d=20, in which the negative $\tilde{u}^*\tilde{\theta}^*$ contour disappear. This is because the positive $\tilde{u}^*$ overwhelms the negative, and hot fluid is mostly associated with vortices in the near wake. At x/d=10, successive $\tilde{v}^*\tilde{\theta}^*$ contours (figure 2c) alternate in sign but their size and magnitude are nearly the same. As x/d increase, the negative $\tilde{v}^*\tilde{\theta}^*$ contour has practically disappeared. The similarity between $\tilde{u}^*\tilde{\theta}^*$ and $\tilde{w}^*\tilde{\theta}^*$ is consistent with the relative closeness between $\tilde{u}^*$ contour and $\tilde{w}^*$ contour. Both of them at x/d=10 are nearly symmetrical about φ=0. Contours of $\tilde{u}^*\tilde{v}^*$ (not shown) and $\tilde{v}^*\tilde{\theta}^*$ (figure 2c) exhibit reasonable similarity at x/d=10. The small value of $\tilde{u}^*\tilde{v}^*$, relative to that for $\tilde{v}^*\tilde{\theta}^*$, implies that vortices transport heat more effectively than momentum, especially at x/d=10, which is consistent with previous results of Matsumura & Antonia (1993).

Contours of correlation between three vorticity components and passive heat ($\tilde{\omega}_x^*\tilde{\theta}^*$, $\tilde{\omega}_y^*\tilde{\theta}^*$, $\tilde{\omega}_z^*\tilde{\theta}^*$) are presented in figure 3a-f (x/d=10 and 20). It can be seen that $\tilde{\omega}_x^*\tilde{\theta}^*$ and $\tilde{\omega}_y^*\tilde{\theta}^*$ have the same magnitude with the coherent heat

fluxes $\tilde{u}^*\tilde{\theta}^*$ and $\tilde{v}^*\tilde{\theta}^*$. The correlation between spanwise vorticity $\tilde{\omega}_z^*$ and heat (figure 3e,f) is considerably larger in magnitude than those of correlations between streamwise and transverse vorticity and heat(figure 3a-d). It should be noted that the decay of $\tilde{\omega}_z^*\tilde{\theta}^*$ is also slower than those of $\tilde{\omega}_x^*\tilde{\theta}^*$ or $\tilde{\omega}_y^*\tilde{\theta}^*$. This behaviour implies that the spanwise structures tend to retain heat, while longitudinal structures play an important role in transferring heat out of spanwise vortices. As *x/d* increases, the rib structures quickly impair and the connection to spanwise structures is greatly weakened.

CONCLUSIONS

Three vorticity components in the intermediate wake of a cylinder have been measured simultaneously. The coherent vorticity field, coherent heat fluxes and correlation of vorticity and passive heat have been calculated based on the phase-averaging method. The $\tilde{\omega}_z^*$ contours display the well-known Kármán vortex street. As *x/d* increases, the strength of the vortex decays and its shape increases. The streamwise variations in the vortex characteristics are accompanied by the disappearance of the positive $\tilde{u}^*\tilde{v}^*$ and negative $\tilde{v}^*\tilde{\theta}^*$. The correlation of three vorticity component and passive heat needs to be further discussed.

REFERENCES

[1] Matsumura, M., Antonia, R.A.(1993). *J. Fluid Mech.*250, 651-668.

[2] Yiu,M.W., Zhou,Y. Zhou, T.(2004). AIAA. 42, 1009-1016.

[3] Zhou,T., Zhou,Y., Yiu,M.W., et al. (2003). *Exp. Fluids*. 35,459-471.

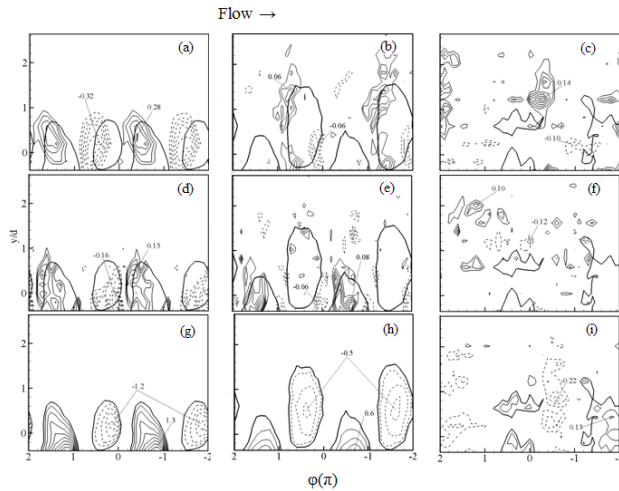[4] Zhou,Y., Zhang, H.J., Yiu,M.W.(2002). *J. Fluid Mech.* 458, 303-332.

Figure 1a-i. Iso-contours of phase-averaged (coherent) vorticities. The thicker solid lines denote the outermost spanwise vorticity contours. $\tilde{\omega}_x^*$:a x/d=10,contour interval=0.04; b 20,0.01; c 40,0.04. $\tilde{\omega}_y^*$: d 10, 0.02; e 20, 0.01; f 40, 0.02. $\tilde{\omega}_z^*$: g 10, 0.1; h 20,0.1; i 40, 0.05.
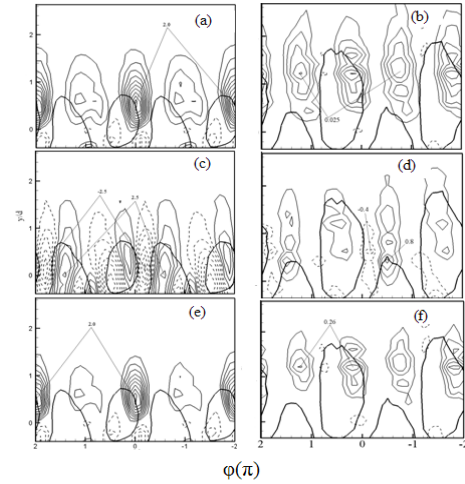

Figure 2 Contours of phase-averaged heat fluxes. $\tilde{u}^*\tilde{\theta}^*$: a x/d=10; b x/d=20; $\tilde{v}^*\tilde{\theta}^*$: c x/d=10; d x/d=20; $\tilde{w}^*\tilde{\theta}^*$: e x/d=10; f x/d=20; Contours intervals are 0.2, 0.5 and 0.2 for (a), (c)and (e) respectively. Contours intervals are 0.05, 0.2 and 0.05 for (b), (d) and (f) respectively. The thicker solid lines denote the outermost vorticity contours in Figure 1
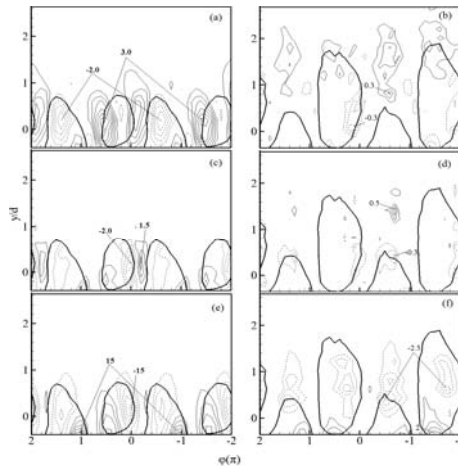

Figure 3 Contours of correlation of vorticity and temperature. $\tilde{\omega}_x^*\tilde{\theta}^*$: a x/d=10; b x/d=20; $\tilde{\omega}_y^*\tilde{\theta}^*$: c x/d=10; d x/d=20; $\tilde{\omega}_z^*\tilde{\theta}^*$: e x/d=10; f x/d=20; Contours intervals are 0.5, 0.5 and 3 for (a), (c)and (e) respectively. Contours intervals are 0.1, 0.1 and 0.5 for (b), (d) and (f) respectively. The thicker solid lines denote the outermost vorticity contours in Figure 1